

# ROVER: Risk-Aware Swarm Robotics MOtion Planner Using Conditional ValuE at Risk\*

Xuru Yang<sup>1</sup>, Yunze Hu<sup>1</sup>, Han Gao<sup>1</sup>, Kang Ding<sup>1</sup>, Pingping Zhu<sup>2</sup>, Ying Sun<sup>3</sup> and Chang Liu<sup>1</sup>

**Abstract**—The field of swarm robotics has attracted considerable interest for its capacity to complete intricate and synchronized tasks. Existing methodologies for motion planning within swarm robotic systems mainly encounter difficulties in scalability and safety guarantee. To address these two limitations, we propose a Risk-aware swarm mOtion planner using conditional ValuE at Risk (ROVER) that systematically modulates the safety and conservativeness and navigates the swarm to the target area through cluttered environments. Our approach formulates a finite-time model predictive control (FTMPC) problem predicated upon the macroscopic state of the robot swarm represented by Gaussian Mixture Model (GMM) and integrates conditional value-at-risk (CVaR) to avoid collision. We leverage the linearized Signed Distance Function for the efficient computation of CVaR concerning the proximity between the robot swarm to obstacles. The key component of this method is implementing CVaR constraint under GMM uncertainty in the FTMPC to measure the collision risk that a robot swarm faces. However, the non-convex constrained FTMPC is nontrivial to solve. To navigate this complexity, we develop a computationally tractable strategy through 1) an explicit linear approximation of the CVaR constraint; and 2) a sequential quadratic programming formulation. Simulations and comparisons with other approaches demonstrate the effectiveness of the proposed method in flexibility, scalability, and risk mitigation.

## I. INTRODUCTION

Large-scale swarm robotic systems comprised of numerous autonomous and interacting robots are witnessing a surge in popularity as a research hot spot, highlighted by their superior robustness and flexibility in applications such as target detection [1], cooperative object transport [2], [3], and search and rescue [4].

This burgeoning interest in swarm robotic systems sets the stage for exploring cooperative and interactive motion planning, the fundamental and vital research problem in swarm robotic systems, which has gained certain progress in fields such as multi-agent reinforcement learning [5]–[7], and optimal control [8]–[10].

\*This work was sponsored by Beijing Nova Program (20220484056) and the National Natural Science Foundation of China (62203018).

<sup>1</sup>Xuru Yang, Yunze Hu, Han Gao, Kang Ding, and Chang Liu are with the Department of Advanced Manufacturing and Robotics, College of Engineering, Peking University, Beijing 100871, China (xuru.yang@stu.pku.edu.cn; hu.yun\_ze@stu.pku.edu.cn; hangao-coe@pku.edu.cn; kangding@stu.pku.edu.cn; changliucoe@pku.edu.cn). All correspondences should be sent to Chang Liu.

<sup>2</sup>Pingping Zhu is with the Department of Computer Sciences and Electrical Engineering (CSEE), Marshall University, Huntington, WV 25755, USA (zhup@marshall.edu).

<sup>3</sup>Ying Sun is with the School of Electrical Engineering and Computer Science, The Pennsylvania State University, State College, PA 16802, USA (ybs5190@psu.edu).

One significant challenge of extending swarm robotic systems into large-scale ones is the scalability of the control mechanism. Present work has revealed two different philosophies, termed as microscopic and macroscopic methods, respectively. The straightforward idea of treating each robot individually and concatenating all state control variables into one state vector aligns with the principles of microscopic approaches. Despite the satisfying performance presented in small and medium-scale robot swarms [11], [12], the dramatic increase in computational demands remains unacceptable for large-scale robotic systems.

Macroscopic approaches provide an alternative to enhance scalability by treating the swarm as an entity instead of focusing on every individual at the planning level. One typical category of macroscopic approaches is based on the mean-field theory [13], [14], representing the swarm state as the average of kinodynamics and cost of all robots, which requires coupling of the macroscopic and microscopic state. Another typical class of macroscopic methods is density control [15]–[18], which models group behavior by distribution and formulates the Monge-Kantorovich optimal control problem over the space of distributions to transform the distribution into the target one, resulting in great improvement in the scalability as the state space is irrelevant with the group size. The key focus of these works is on theoretically designing algorithms with low computational cost to find optimal density control input, especially in high-dimensional spaces. However, these works all overlook the design of obstacle avoidance and greatly simplify the motion model, which makes them relatively detached from practical applications.

Recently, hierarchical approaches that integrate both the advantages of macroscopic and microscopic concepts are receiving increased attention. These approaches balance scalability and practicality by decoupling the macroscopic planning from the microscopic control level that considers real-world constraints. The adaptive distributed optimal control (ADOC) presented by [19], approximated obstacles in the macroscopic planning phase with grid maps and penalized the collision inner product within the objective function, which fails to guarantee collision-free macroscopic trajectories. [20] proposed a multi-level hierarchical framework, where all cliques are seen as individuals of their parent level. This work extends the scale of the multi-robot systems into a million level but in the scenario of circular obstacles and simplified kinematic models. [21] and [22] combined the macroscopic planning and microscopic control. The planning stage provides the robots with local goals

or reference trajectories, while the control stage allows the robots to execute microscopic control distributively to track the local goal or trajectories given by the planning stage. An evident drawback of these approaches lies in the poor flexibility as the whole swarm is restricted into certain formations, which prevents the swarm from making splitting and merging behavior, posing significant planning challenges when navigating through obstacle-cluttered environments.

Apart from the scalability issue, safety guarantee in swarm motion planning also poses an indispensable challenge to the wide application of large-scale swarm robotic systems. A widely used risk measurement is chance constraint, aiming to limit the risk occurring probability under a pre-defined threshold [23], [24]. A concept associated with this is value-at-risk (VaR). While chance constraint controls the probability of constraint violation, VaR denotes the risk quantile that arises at a specified probability. Another risk measurement, namely conditional value-at-risk (CVaR), measures the expected risk that would occur beyond the VaR level, which enables CVaR to better recognize the long-tail distribution of risks than constraint-based methods and VaR. Given the desirable properties previously discussed, implementations of CVaR in motion planning under environment uncertainty or imperfect robot models have been increasingly witnessed in either single or small-scale robotic systems in the past few years. [25] proposed a risk-aware planning framework incorporating CVaR that modifies different sources of traversability risk measured by Gaussian uncertainty [26]. [27] adopted the CVaR constraints to represent the collision risk in an uncertain environment with moving obstacles and later extended this work into a distributionally robust optimization framework in an uncertainty ambiguity set defined by Wasserstein distance [28]. Similar to data-driven methods [29], these two works approximate CVaR through sampling, which leads to substantial computational cost and sample-size-dependent results. Despite the progress made, existing work predominantly focuses on modeling the uncertainty inherent in either individual or small-scale robotic systems, rather than characterizing the risk across the traverse from the macroscopic aspect of robot swarms, which prohibits the scalability of CVaR-constrained programming.

To address these two difficulties, we propose a risk-aware swarm robotics motion planner using conditional value at risk (ROVER). The specific contributions of this work can be summarized as follows:

- We propose a hierarchical motion planning framework for robot swarm. Specifically, the macroscopic planning state of the swarm, represented as Gaussian Mixture Models (GMMs), is formulated as a finite-time model predictive control (FTMPC) problem, which integrates CVaR as risk measurement to generate collision-free trajectories in obstacle-cluttered environments.
- We propose to linearize the Signed Distance Function (SDF) to obtain the distance distribution between the robot swarm and obstacles, which enables the risk-aware formulation of the swarm utilizing CVaR.
- We analyze the properties of CVaR under GMM un-

certainty (GMM-CVaR). By overapproximating GMM-CVaR, we propose a convergent sequential optimization algorithm to tackle the computational burden of the original Nonlinear Programming (NLP). To the best of our knowledge, this paper is the first that applies GMM-CVaR to swarm motion planning and achieves efficient online solutions.

- We validate the flexibility, scalability, and risk control capacity of ROVER through extensive simulations. Comparisons with representative benchmark methods demonstrate the outstanding performance of our approach.

## II. BACKGROUND AND PROBLEM FORMULATION

In this section, we provide an overview of the important preliminaries including Wasserstein metric, signed distance function, and CVaR, followed by the problem formulation. For simplicity, we will abbreviate ‘‘Gaussian component’’ as ‘‘GC’’ in below, and the index set  $\{1, 2, \dots, N\}$  for any  $N \in \mathbb{N}_+$  is briefly denoted as  $\underline{N}$ .

### A. Wasserstein Metric

The Wasserstein metric measures the distance between two probability distributions on a given metric space, and is widely used in the optimal transport problems [30]. We first consider two Gaussian PDFs denoted by  $g_1 = \mathcal{N}(\boldsymbol{\mu}_1, \boldsymbol{\Sigma}_1) \in \mathcal{P}(\mathbb{R}^d)$  and  $g_2 = \mathcal{N}(\boldsymbol{\mu}_2, \boldsymbol{\Sigma}_2) \in \mathcal{P}(\mathbb{R}^d)$ , where  $\mathcal{P}(\Omega)$  denotes the set of all the probability distributions defined on the sample space  $\Omega$ . The Wasserstein metric between  $g_1$  and  $g_2$  can be efficiently calculated as follows [31]:

$$W_2(g_1, g_2) = \left\{ \|\boldsymbol{\mu}_1 - \boldsymbol{\mu}_2\|^2 + \text{tr} \left[ \boldsymbol{\Sigma}_1 + \boldsymbol{\Sigma}_2 - 2 \left( \boldsymbol{\Sigma}_1^{1/2} \boldsymbol{\Sigma}_2 \boldsymbol{\Sigma}_1^{1/2} \right)^{1/2} \right] \right\}^{1/2}, \quad (1)$$

where  $\text{tr}(\cdot)$  indicates the trace operator, and  $\|\cdot\|$  denotes the 2-norm. Further, the Wasserstein metric of two GMMs can be approximated utilizing eq. (1) [31]. Specifically, consider two GMMs with  $N_1$  and  $N_2$  GCs denoted by  $\wp_1 = \sum_{i=1}^{N_1} \omega_1^i g_1^i$ ,  $\wp_2 = \sum_{j=1}^{N_2} \omega_2^j g_2^j$ , where  $g_1^i, g_2^j$  denote the  $i$ th and  $j$ th GCs of  $\wp_1$  and  $\wp_2$ , respectively, and  $\omega_1^i, \omega_2^j$  denote their corresponding weights that satisfy  $\sum_{i=1}^{N_1} \omega_1^i = \sum_{j=1}^{N_2} \omega_2^j = 1$ .

The approximated Wasserstein metric  $W_2(\wp_1, \wp_2)$  can be formulated as:

$$W_2(\wp_1, \wp_2) \triangleq \left\{ \min_{\pi \in \Pi(\boldsymbol{\omega}_1, \boldsymbol{\omega}_2)} \sum_{i=1}^{N_1} \sum_{j=1}^{N_2} [W_2(g_1^i, g_2^j)]^2 \pi(i, j) \right\}^{1/2}. \quad (2)$$

where  $\boldsymbol{\omega}_1 = [\omega_1^1, \dots, \omega_1^{N_1}]$ ,  $\boldsymbol{\omega}_2 = [\omega_2^1, \dots, \omega_2^{N_2}]$ . The  $\Pi(\boldsymbol{\omega}_1, \boldsymbol{\omega}_2) \subset \mathcal{P}([0, 1]^{N_1} \times [0, 1]^{N_2})$  is comprised of all the joint probability mass functions  $\pi(\boldsymbol{x}_1, \boldsymbol{x}_2)$  whose marginals PMFs are  $\boldsymbol{\omega}_1$  and  $\boldsymbol{\omega}_2$ , i.e.,

$$\int_{\boldsymbol{x}_i \in [0, 1]^{N_i}} \pi(\boldsymbol{x}_1, \boldsymbol{x}_2) d\boldsymbol{x}_i = \boldsymbol{\omega}_{2-i}, i = 1, 2. \quad (3)$$

and  $\pi(i, j)$  is the joint probability mass function between the  $i$ th GC weight in  $\wp_1$  and the  $j$ th GC weight in  $\wp_2$ .

### B. Signed Distance Function (SDF)

The SDF measures the orthogonal distance between a point and the boundary of a set in a metric space with the sign indicating whether or not the point is in the interior of the set. In particular, the SDF between a point  $\mathbf{p} \in \mathbb{R}^2$  and an obstacle  $\mathcal{O}_i \subset \mathbb{R}^2$  can be calculated as follows

$$sd(\mathbf{p}, \mathcal{O}_i) = \begin{cases} -d(\mathbf{p}, \partial\mathcal{O}_i), & \mathbf{p} \in \mathcal{O}_i \\ d(\mathbf{p}, \partial\mathcal{O}_i), & \mathbf{p} \notin \mathcal{O}_i \end{cases}, \quad (4)$$

where  $d(\mathbf{p}, \partial\mathcal{O}_i)$  is the minimum distance from  $\mathbf{p}$  to the boundary of  $\mathcal{O}_i$ , noted as  $\partial\mathcal{O}_i$ . The closest point to  $\mathbf{p}$  on  $\partial\mathcal{O}_i$  is denoted as  $\mathbf{o}_i^*$ , and the normal vector along the SDF direction can be calculated as follows:

$$\mathbf{n} = \text{sgn}(sd(\mathbf{p}, \mathcal{O}_i)) \cdot (\mathbf{p} - \mathbf{o}_i^*) / \|\mathbf{p} - \mathbf{o}_i^*\|, \quad (5)$$

where  $\text{sgn}(\cdot)$  is the sign function. The calculation of SDF and its corresponding normal vector  $\mathbf{n}$  can be efficiently performed using the Gilbert–Johnson–Keerthi (GJK) algorithm [32] Expanding Polytope Algorithm (EPA) [33].

### C. VaR and CVaR

The VaR represents the minimum possible value of risk that can be achieved given a specific risk tolerance level. Specifically, the VaR of a random variable  $\zeta$  under risk tolerance level  $\alpha \in (0, 1]$  is defined as

$$VaR_\alpha(\zeta) = \min \{z | Pr(\zeta \leq z) \geq 1 - \alpha\}, \quad (6)$$

where  $Pr(\cdot)$  denotes the probability. Then according to [34], the CVaR of random variable  $\zeta$  with a continuous distribution is defined as

$$CVaR_\alpha(\zeta) = \min_{z \in \mathbb{R}} \mathbb{E}[z + (\zeta - z)^+ / \alpha] = \mathbb{E}[\zeta | \zeta \geq VaR_\alpha(\zeta)], \quad (7)$$

where  $(\cdot)^+ = \max(\cdot, 0)$ , and  $\mathbb{E}$  is the expectation operator.

Let  $\phi(\cdot)$  and  $\Phi(\cdot)$  denote the PDF and the cumulative distribution function (CDF) of a standard normal distribution, respectively. The CVaR of a Gaussian random variable  $\zeta \sim \mathcal{N}(\mu, \sigma^2)$  has the following closed-form expression [26]

$$CVaR_\alpha(\zeta) = \mu + \sigma \phi(\Phi^{-1}(1 - \alpha)) / \alpha. \quad (8)$$

### D. Problem Formulation

Consider the workspace  $\mathcal{W} \subset \mathbb{R}^2$  that contains a robot swarm consisting of  $N_r$  robots and  $N_o$  static obstacles  $\mathcal{O}_i \subset \mathcal{W}, i \in \underline{N}_o$ . Let  $\mathcal{O} = \bigcup_{i=1}^{N_o} \mathcal{O}_i$  represent the union of all obstacles. For simplicity,  $\mathcal{O}_i$  is assumed to be convex. In the context of non-convex obstacles, the convex hull or convex decomposition can be employed to ascertain convex obstacles.

The macroscopic state of the swarm can be represented by a random variable  $\mathbf{X}$  whose PDF indicates the density distribution of robots across the workspace. Given the universal approximation property of Gaussian Mixture Models (GMMs), we choose a GMM  $\wp_k = \sum_{j=1}^{N_k} \omega_k^j g_k^j$  with  $\sum_{j=1}^{N_k} \omega_k^j = 1$  from the GMM distribution space  $\mathcal{G}(\mathcal{W})$  to represent the macroscopic state of the robot swarm at time step  $k$ , i.e.,  $\mathbf{X}(k) \sim \wp_k$ . Here  $N_k$  denotes the number of GCs in the GMM and  $g_k^j$  is the  $j$ th Gaussian distribution with mean  $\boldsymbol{\mu}_k^j$ , covariance matrix  $\boldsymbol{\Sigma}_k^j$  and a weight  $\omega_k^j > 0$ .

The position of every single robot can be treated as a sample from the GMM chosen above. Without loss of generality, the motion model of the robots is formulated as

$$\begin{aligned} \mathbf{x}_i(k+1) &= f(\mathbf{x}_i(k), \mathbf{u}_i(k)) + \mathbf{w}(k), \\ k &= 0, 1, \dots, T_f, i = 1, 2, \dots, N_r, \end{aligned} \quad (9)$$

where  $\mathbf{x}_i(k) \in \mathbb{R}^{n_x}$  and  $\mathbf{u}_i(k) \in \mathbb{R}^{n_u}$  denote the state and control input for every single robot at time step  $k$ ,  $T_f$  is the terminal time step, and  $f(\cdot, \cdot)$  is the robot motion function. The  $\mathbf{w}(k)$  represents zero-mean Gaussian white process noise with covariance matrix  $\boldsymbol{\Sigma}_0$ .

The swarm motion planning problem aims to safely transport the robots from an initial area to a designated region in obstacle-cluttered environments. This task is addressed through a two-stage hierarchical strategy involving a macroscopic planning stage and a microscopic control stage.

The macroscopic planning stage is formulated as a swarm PDF optimal transport problem from an initial distribution  $\wp_0 \in \mathcal{G}(\mathcal{W})$  to a target distribution  $\wp_{target} \in \mathcal{G}(\mathcal{W})$  while minimizing the total transport cost and satisfying a set of collision avoidance constraints. The optimal transport problem at time step  $k$  can be formulated into the problem (P0) as follows:

$$\min_{\wp_{k+1}, \dots, \wp_{T_f}} J \triangleq \sum_{p=k}^{T_f-1} \lambda_p W_2(\wp_p, \wp_{p+1}) \quad (10a)$$

$$s.t. \quad CVaR_\alpha(-sd(\mathbf{X}(p+1), \mathcal{O}_i)) < \epsilon, \quad (10b)$$

$$f_i(\wp_p) < \epsilon, \quad (10c)$$

$$p = k, k+1, \dots, T_f, i \in \underline{N}_o, \quad (10d)$$

where the optimization objective is the sum of the Wasserstein distance between consecutive PDFs from the current time step to the terminal time step with corresponding weight coefficients  $\lambda_p > 0$ . The constraint eq. (10b) limits the maximum expected distance of intersection between the swarm PDF and obstacles. Taking the opposite sign of SDF is performed to accommodate the definition of CVaR. Details regarding  $sd(\cdot, \cdot)$  will be provided in Sec. III-B. Equation (10c) constrains the probability density of  $\wp_p$  under a specified threshold  $\epsilon$ , which ensures that the robots do not come too close to each other. The  $f_i(\cdot)$  is a linear function. A more detailed elaboration will be presented in Sec. III-A.

In the microscopic control stage, individual robots determine control inputs using the artificial potential field (APF) method to keep track of the swarm PDF given by the macroscopic planning stage and avoid collisions with static obstacles and other robots. Since the microscopic control falls beyond the scope of this work, interested readers are encouraged to consult [35] for more comprehensive details.

## III. METHODOLOGY

### A. Macroscopic Planning Formulation

The proposed PDF optimal transport problem in eq. (10) is an infinite-dimensional optimization problem, which is theoretically solvable but computationally prohibitive. Thus, we proposed two approximations to simplify the problem.

In the first approximation, we uniformly discretize the planning space and establish a specific set  $\mathcal{C}$  of GCs with uniform covariance matrices and mean positions constrained to discrete points. Every GC in  $\mathcal{C}$  is identified by an index, and we denote the index set as  $\mathcal{I} \subset \mathbb{N}_+^{|\mathcal{C}|}$ . With this approximation, we propose the following two assumptions:

**Assumption 1.** All GCs of the GMM in the planning process can only be chosen from  $\mathcal{C}$ , i.e.,  $g_k^j \in \mathcal{C}, j \in \underline{N}_k, k \in \underline{T}_f$ .

**Assumption 2.** Between consecutive planning steps, GCs can be only transported to the GCs within a predefined transport radius measured by the Wasserstein Metric.

In the second approximation, we proposed to split the transport costs into stage cost and terminal cost utilizing the framework of MPC. The stage cost represents the transport cost within the MPC planning horizon, while the terminal cost is defined as the cost from the last step in the planning horizon to the terminal step  $T_f$ . To calculate the terminal cost, we propose an assumption as follows:

**Assumption 3.** The GCs of the GMM from the last step in the planning horizon to  $T_f - 1$  do not split or merge. Transformation into the target distribution is conducted in the terminal step  $T_f$ .

With the help of these two manipulations, the optimal transport problem (P0) is recast within the MPC framework into (P) as follows:

$$\begin{aligned} \min_{\pi(\cdot, \cdot)} J \triangleq & \sum_{p=1}^h \sum_{i=1}^{N_{k+p-1}} \sum_{j=1}^{N_{k+p}} \lambda_{k+p-1} W_2^2(g_{k+p-1}^i, g_{k+p}^j) \pi_{k+p-1}(i, j) \\ & + \sum_{m=1}^{N_{k+h}} \sum_{n=1}^{N_{target}} \lambda_{k+h} \mathcal{Q}_{k+h}(m, n) \pi_{k+h}(m, n) \end{aligned} \quad (11a)$$

$$s.t. \quad \omega_{k+p-1}^i = \sum_{j=1}^{N_{k+p}} \pi_{k+p-1}(i, j), \quad i \in \underline{N_{k+p-1}} \quad (11b)$$

$$\omega_{k+p}^j = \sum_{i=1}^{N_{k+p-1}} \pi_{k+p-1}(i, j), \quad j \in \underline{N_{k+p}} \quad (11c)$$

$$\omega_{k+h}^m = \sum_{n=1}^{N_{target}} \pi_{k+h}(m, n), \quad m \in \underline{N_{k+h}} \quad (11d)$$

$$\omega_{target}^n = \sum_{m=1}^{N_{k+h}} \pi_{k+h}(m, n), \quad n \in \underline{N_{target}} \quad (11e)$$

$$\sum_{i=1}^{N_{k+p-1}} \sum_{j=1}^{N_{k+p}} f_l(g_{k+p}^j) \pi_{k+p-1}(i, j) < \varepsilon \quad (11f)$$

$$CVaR_\alpha(-sd(\mathbf{X}(k+p), \mathcal{O}_\iota)) < \epsilon, \quad (11g)$$

$$p \in \underline{h}, \quad \iota \in \underline{N_o} \quad (11h)$$

where  $h$  is the planning horizon and the subscripts of  $g$  denote the time step. The optimization variable  $\pi(\cdot, \cdot) = [\pi_k(\cdot, \cdot), \pi_{k+1}(\cdot, \cdot), \dots, \pi_{k+h}(\cdot, \cdot)]$  is a stack of joint Probability Mass Functions (PMFs) whose marginal PMFs are denoted by eqs. (11b) to (11e). As an example,  $\pi_k(i, j)$  represents the weight transported from  $g_k^i$  to  $g_{k+1}^j$ .

The former half of eq. (11a) represents the stage cost with weights  $\lambda_{k:k+h-1}$ , while the latter half represents the

terminal cost, with a weight  $\lambda_{k+h}$ . As assumption 1 and assumption 2 hold, within the planning horizon, all the GCs of the GMM, noted as  $\mathcal{G}_{k+p} \subset \mathcal{C}$ , and the component number  $N_{k+p} \in \mathbb{N}_+$  can be predetermined, and the squared terms of  $W_2(\cdot, \cdot)$  in the stage cost can be calculated offline. For the terminal cost, we adopt the transport policy as in assumption 3 and leverage a directed graph  $\mathbf{G}$  whose vertices are GCs from  $\mathcal{C}$  and weights are determined by the Wasserstein distance between the two vertices and their respective Gaussian CVaR, which represents the risk of this trajectory. Then, the cost term  $\mathcal{Q}_{k+h}(m, n)$  in the terminal cost can be computed by applying a shortest-path-planning algorithm on  $\mathbf{G}$  in advance. Therefore, the cost function eq. (11a) is linear w.r.t.  $\pi(\cdot, \cdot)$ .

Similarly, the constraint eq. (11f) is linear w.r.t.  $\pi(\cdot, \cdot)$ . But the formulation of constraint eq. (11g) remains unclear. The specific handling of this constraint will be elaborated in Sec. III-B and Sec. III-C. Note that the constraints eqs. (11f) and (11g) are only applied to steps in the planning horizon, not steps afterward.

## B. SDF under GMM Uncertainty

The collision avoidance constraint eq. (11g) involves SDF between the swarm PDF and the obstacles. Taking the GMM representation of the robot swarm into account, we consider a GMM random variable  $\mathbf{X} \sim \sum_{j=1}^N \omega_j \mathcal{N}(\boldsymbol{\mu}_j, \boldsymbol{\Sigma}_j)$  and derive the stochastic SDF distribution between the swarm GMM and an obstacle  $\mathcal{O}_i$ , which is denoted as  $sd(\mathbf{X}, \mathcal{O}_i)$ .

For simplicity, we first consider the  $j$ th GC of a GMM denoted as  $\mathbf{X}^j \sim \mathcal{N}(\boldsymbol{\mu}_j, \boldsymbol{\Sigma}_j)$  and its corresponding  $sd(\mathbf{X}^j, \mathcal{O}_i)$ . Utilizing the EPA or GJK algorithm and eq. (5), the deterministic SDF between the mean position and an obstacle  $\mathcal{O}_i$ , denoted by  $sd(\boldsymbol{\mu}_j, \mathcal{O}_i)$ , and the corresponding normal vector  $\mathbf{n}_j$  can be calculated.

The  $sd(\mathbf{X}^j, \mathcal{O}_i)$  can be subsequently approximated by the first-order Taylor expansion as follows,

$$sd(\mathbf{X}^j, \mathcal{O}_i) \approx sd(\boldsymbol{\mu}_j, \mathcal{O}_i) + \nabla sd(\mathbf{X}^j, \mathcal{O}_i)|_{\mathbf{X}^j=\boldsymbol{\mu}_j} (\mathbf{X}^j - \boldsymbol{\mu}_j), \quad (12)$$

where  $\nabla sd(\mathbf{X}^j, \mathcal{O}_i)|_{\mathbf{X}^j=\boldsymbol{\mu}_j} = \mathbf{n}_j^T$ . The reasonableness of this approximation stems from the assumption, inspired by [36], that when calculating  $sd(\mathbf{X}^j, \mathcal{O}_i)$ , the closest point  $\mathbf{o}_i^*$  and the normal vector  $\mathbf{n}_j$  remain unchanged for any sample  $\mathbf{X}^j \sim \mathcal{N}(\boldsymbol{\mu}_j, \boldsymbol{\Sigma}_j)$ . The approximation error is acceptable when  $\mathbf{X}^j$  lies in the neighborhood of  $\boldsymbol{\mu}_j$ . Notice that  $sd(\mathbf{X}^j, \mathcal{O}_i)$  is a Gaussian random variable as a result of the linear transformation of a Gaussian random variable  $\mathbf{X}^j$ , i.e.,

$$sd(\mathbf{X}^j, \mathcal{O}_i) \sim \mathcal{N}(sd(\boldsymbol{\mu}_j, \mathcal{O}_i), \mathbf{n}_j^T \boldsymbol{\Sigma}_j \mathbf{n}_j). \quad (13)$$

Next, we further derive  $sd(\mathbf{X}, \mathcal{O}_i)$  based on eq. (13). The derivation begins with the following proposition:

**Proposition 1.** The distribution  $\sum_{j=1}^N \omega_j Pr(sd(\mathbf{X}^j, \mathcal{O}_i))$  and distribution  $Pr(sd(\mathbf{X}, \mathcal{O}_i))$  are equal.

The proof can be found in Sec. V-A.

Proposition 1 yields that  $sd(\mathbf{X}, \mathcal{O}_i)$  follows a GMM distribution:

$$sd(\mathbf{X}, \mathcal{O}_i) \sim \sum_{j=1}^N \omega_j \mathcal{N}(sd(\boldsymbol{\mu}_j, \mathcal{O}_i), \mathbf{n}_j^T \boldsymbol{\Sigma}_j \mathbf{n}_j). \quad (14)$$

Therefore, the  $sd(\cdot, \cdot)$  in eq. (11g) can be calculated by  $sd(\mathbf{X}, \mathcal{O}_i) = \sum_{j=1}^N \omega_j sd(\mathbf{X}^j, \mathcal{O}_i)$  utilizing eq. (12).

### C. CVaR Under GMM Uncertainty

The collision avoidance constraints eq. (11g) involve CVaR of a GMM random variable, for which there is currently no analytical expression available. Therefore, we first propose a proposition concerning CVaR of a GMM random variable.

**Proposition 2.** *The CVaR of a GMM random variable  $Y$  at risk acceptance level  $\alpha$  can be represented by the summation of CVaRs of the Gaussian component  $Y^j$  of  $Y$  at the risk acceptance level  $\alpha_j$ :*

$$CVaR_\alpha(Y) = \frac{1}{\alpha} \sum_{j=1}^N \omega_j \alpha_j CVaR_{\alpha_j}(Y^j), \quad (15)$$

where  $\omega_j$  denotes the weight of  $Y^j$ , and  $\alpha_j$  is the tail probability of the  $Y^j$  distribution at the  $VaR_\alpha(Y)$  quantile, i.e.,  $\alpha_j = \int_{VaR_\alpha(Y)}^{+\infty} p(Y^j) dy$ . Besides, there exists relationship between  $\alpha$  and  $\alpha_j$  denoted as  $\alpha = \sum_{j=1}^N \omega_j \alpha_j$ .

The proof is given in Sec. V-B.

In proposition 2, by defining  $Y = -sd(\mathbf{X}, \mathcal{O}_i)$  and  $Y^j = -sd(\mathbf{X}^j, \mathcal{O}_i)$ , the constraint eq. (11g) can be given as

$$CVaR_\alpha(Y) = \frac{1}{\alpha} \sum_{j=1}^N \omega_j \alpha_j CVaR_{\alpha_j}(Y^j) < \epsilon. \quad (16)$$

Although  $CVaR_{\alpha_j}(Y^j)$  can be explicitly expressed by eq. (8),  $\alpha_j$  relating with  $VaR_\alpha(Y)$  is still coupled with the weights of GCs, which renders eq. (11g) a nonlinear constraint. To tackle the prohibitively high computational cost arising from the nonlinear constraint, a computationally efficient algorithm is proposed in the next section.

### D. Sequential Quadratic Programming (SQP)

We propose to linearize the constraint of  $CVaR_\alpha(Y)$  to address the computational challenges. [37] demonstrate that  $CVaR_\alpha(Y)$  exhibits concavity w.r.t. the weight vector  $\boldsymbol{\omega} = [\omega_1, \omega_2, \dots, \omega_N]$ . Thus, the first-order Taylor expansion of  $CVaR_\alpha(Y)$  w.r.t.  $\boldsymbol{\omega}$  is always an upper bound of  $CVaR_\alpha(Y)$ , which represents a more conservative approximation of the collision avoidance constraint.

Applying Danskin's theorem [38] to the definition of CVaR denoted as eq. (7) shows that  $CVaR_\alpha(Y)$  is differentiable at  $\boldsymbol{\omega}$ . And the gradient of  $CVaR_\alpha(Y)$  w.r.t.  $\boldsymbol{\omega}$  represented by

$$\nabla_{\boldsymbol{\omega}} CVaR_\alpha(Y) = \left[ \frac{\partial CVaR_\alpha(Y)}{\partial \omega_1}, \dots, \frac{\partial CVaR_\alpha(Y)}{\partial \omega_N} \right]^T \quad (17)$$

can be computed by

$$\frac{\partial CVaR_\alpha(Y)}{\partial \omega_j} = \frac{\alpha_j}{\alpha} CVaR_{\alpha_j}(Y^j) - \frac{\alpha_j}{\alpha} VaR_\alpha(Y). \quad (18a)$$

A detailed derivation can be referred to Sec. V-C

To facilitate a more comprehensive explanation and better utilize the above-mentioned properties of CVaR, we propose a *flow variable*  $\mathbf{F}_{I_k, I_{k+1}, \dots, I_{k+h}, I_{targ}} \in \mathbb{R}_+$ . Specifically,  $\mathbf{F}_{I_k, I_{k+1}, \dots, I_{k+h}, I_{targ}}$  represents the weight of the PDF transported along a specific route identified by a set of GC indices  $I_k, I_{k+1}, \dots, I_{k+h}, I_{targ} \in \mathcal{I}$ , where the subscript corresponds to different time steps. For simplicity, we denote the flow vector  $\mathbf{F}$  as the combination of all the flow variables, and it is worth noting that  $\mathbf{F}$  is an equivalent form of  $\boldsymbol{\omega}$ . Furthermore, we define the notation  $\mathbf{F}_{I_{k+p}=j} \in \mathbb{R}_+^{\prod_{i=1, i \neq p}^{N_{targ}} N_{k+i}}$  as a vector combining all the flow variables that pass through the  $j$ th GC at the time step  $k+p$ .

With the flow variable representation, the weight of the  $j$ th GC can be rewritten as the sum of all flow variables that pass through the  $j$ th GC, i.e.,

$$\begin{aligned} \omega_{k+p}^j &= \sum \mathbf{F}_{I_{k+p}=j} \quad p = 1, 2, \dots, h \\ \omega_{targ}^j &= \sum \mathbf{F}_{I_{targ}=j}. \end{aligned} \quad (19)$$

where the  $\sum$  denotes the summation of all the variables in the vector. Further, the optimization variable  $\boldsymbol{\pi}(\cdot, \cdot)$  presented in (P) can also be transformed into the sum of all the flow variables passing through two particular components at consecutive two steps:

$$\pi_{k+p-1}(m, n) = \begin{cases} \sum \mathbf{F}_{I_{k+p-1}=m, I_{k+p}=n}, & p = 1, \dots, h \\ \sum \mathbf{F}_{I_{k+h}=m, I_{targ}=n}, & p = h + 1 \end{cases}, \quad (20)$$

Since  $\boldsymbol{\omega}$  holds a linear relationship with flow variables, the concavity of the function  $CVaR_\alpha(Y)$  w.r.t.  $\mathbf{F}$  can also be derived. Based on the chain rule, the gradient of  $CVaR_\alpha(Y(k+p))$  denoted by  $\nabla_{\mathbf{F}} CVaR_\alpha(Y(k+p))$  can be obtained with each partial derivative from the gradient vector determined by

$$\frac{\partial CVaR_\alpha(Y(k+p))}{\partial \mathbf{F}_{I_{k+p}=j}(i)} = \frac{\partial CVaR_\alpha(Y(k+p))}{\partial \omega_{k+p}^j}, \forall i. \quad (21)$$

where  $\mathbf{F}_{I_{k+p}=j}(i)$  denote the  $i$ th element of  $\mathbf{F}_{I_{k+p}=j}$ . Drawing upon the insights presented by [39], we proposed to address the non-convex constrained optimization problem (P) by sequentially solving a series of strongly convex optimization subproblems  $(P^v)$ ,  $v \in \mathbb{N}_+$ . For each subproblem  $(P^v)$ , we linearize the  $CVaR_\alpha(Y(k+p))$  constraint using the first-order Taylor expansion at a feasible solution of  $(P^v)$   $\mathbf{F}^v$  as:

$$\begin{aligned} CVaR_\alpha(Y(k+p)) &= CVaR_\alpha(Y_v(k+p)) \\ &+ \nabla_{\mathbf{F}}^T CVaR_\alpha(Y(k+p))|_{\mathbf{F}=\mathbf{F}^v} (\mathbf{F} - \mathbf{F}^v) \end{aligned} \quad (22a)$$

The subproblem  $(P^v)$  at each iteration is as follows:

$$\min_{\mathbf{F}} J + \frac{\tau}{2} \|\mathbf{F} - \mathbf{F}^v\|^2 \quad (23a)$$

$$s.t. \quad (11b) - (11f), (20), (11h), \quad (23b)$$

$$eq. (22a) < \epsilon, \quad (23c)$$

where eq. (23a) is a strongly convex approximation of  $J$  due to the regularization term with weight  $\tau > 0$ . The subproblems ( $P^v$ ) are Quadratic Programming (QP) problems, which enable high computational efficiency in the solution process. Due to the concavity of CVaR, the design of linearized constraint eq. (23c) ensures that the feasible domain of ( $P^v$ ) is a closed, convex, inner approximation of the feasible domain of ( $P$ ). Consequently, the limit point of the sequence  $\mathbf{F}^v$  corresponds to the stationary points of ( $P$ ) as proved in [39].

The detailed execution of the proposed SQP is presented in Alg. 1. Every iteration involves first searching the  $VaR_\alpha(Y(k+p))$  and  $\alpha_{1:N_{k+p}}$  (line 5) given the GMM  $Y(k+p)$ , which is derived from  $\mathbf{F}^v$  and  $\mathcal{G}_{k+p}$ . Specifically, the main process of VARSEARCH is a binary search conducted on the CDF of  $Y(k+p)$  given the risk acceptance level  $\alpha$ , and  $\alpha_{1:N_{k+p}}$  is calculated by querying the individual CDF of  $Y^j(k+p)$  on the quantile  $VaR_\alpha(Y(k+p))$ . Then we compute the CVaR of  $Y(k+p)$  and its gradient (lines 6 and 7), which is required for the linearization of the  $CVaR_\alpha(Y(k+p))$  constraint (line 8). Then we solve ( $P^v$ ) and update  $\mathbf{F}^v$  with the step size  $\gamma^v$  in line 12. This algorithm is sequentially executed until  $\mathbf{F}^v$  meets the convergence condition.

---

#### Algorithm 1 SQP

---

**Input:** a feasible  $\mathbf{F}^v, \mathcal{G}_{k+1:h}, \mathcal{O}, \alpha, \theta > 0, \eta > 0$

- 1: Initialization:  $v \leftarrow 0$
- 2: **while**  $\|\mathbf{F}^v - \mathbf{F}^{v-1}\| > \eta$  or  $v == 0$  **do**
- 3:   **for**  $i = 1$  to  $N_o$  **do**
- 4:     **for**  $p = 1$  to  $h$  **do**
- 5:       compute  $VaR_\alpha(Y(k+p))$  and  $\alpha_{1:N_{k+p}}$  with VARSEARCH( $\mathbf{F}^v, \mathcal{G}_{k+p}, \mathcal{O}_i, \alpha, \theta$ )
- 6:       compute  $CVaR_\alpha(Y(k+p))$  based on eqs. (8) and (15)
- 7:       compute  $\nabla_{\mathbf{F}} CVaR_\alpha(Y(k+p))|_{\mathbf{F}=\mathbf{F}^v}$  based on eqs. (18a) and (21)
- 8:       linearize  $CVaR_\alpha(Y(k+p))$  based on eq. (22a)
- 9:     **end for**
- 10:    **end for**
- 11:    solve ( $P^v$ ) to find  $\mathbf{F}^{v*}$
- 12:     $\mathbf{F}^{v+1} \leftarrow \mathbf{F}^v + \gamma^v(\mathbf{F}^{v*} - \mathbf{F}^v)$ , where  $\gamma^v \in (0, 1]$
- 13:     $v \leftarrow v + 1$
- 14: **end while**
- 15: compute  $\omega_{k+1}$  from  $\mathbf{F}^{v*}$  based on eq. (19)

**Output:**  $\omega_{k+1}$

---

## IV. SIMULATION AND RESULTS

The proposed method ROVER is evaluated in swarm motion planning task simulations. The workspace  $\mathcal{W}$  is a  $[0, 200] \times [0, 160]m^2$  area with static obstacles. The initial distribution of the swarm consists of four GCs with a shared covariance matrix  $\Sigma = 100\mathbf{I}_2$ , where  $\mathbf{I}_2$  denotes  $2 \times 2$  identity matrix. Other parameters are  $\mu_1 = [25, 35], \omega_1 = 0.25$ ,  $\mu_2 = [25, 55], \omega_2 = 0.375$ ,  $\mu_3 = [25, 115], \omega_3 =$

$0.1875$ ,  $\mu_4 = [25, 135], \omega_4 = 0.1875$ . The target distribution is composed of three GCs with parameters  $\mu_1 = [175, 120], \omega_1 = 0.25$ ,  $\mu_2 = [175, 60], \omega_2 = 0.375$ ,  $\mu_3 = [175, 120], \omega_3 = 0.375$  and an identical covariance matrix  $\Sigma = 100\mathbf{I}_2$ . The GC set  $\mathcal{C}$  is predefined by taking the mean of each Gaussian on fixed grids, where the X coordinates range from 5 to 195 and the Y coordinates range from 5 to 155, with a discretization interval of 10. Consequently, the set  $\mathcal{C}$  comprises a total of  $20 \times 16 = 320$  GCs, each with the same covariance matrix  $\Sigma_c = 50\mathbf{I}_2$ .

We set the discretization time interval  $\Delta t$  to  $0.1s$  and a maximal robot speed to  $1.5m/s$ . Additionally, in the analysis of inter-robot distance and distance between robots and obstacles, the radius of robots is assumed to be  $0.15m$ .

For the constraint formulation,  $\alpha$  and  $\epsilon$  are set to 0.05 and -0.2 respectively. In the objective function, we set  $\lambda_{k+h}$  to 3,  $\lambda_{k+p-1}$  to 1 and  $\tau$  to 0.001. The SQP step size is set as  $\gamma^v = 1$ . The  $\eta$  in the convergence condition is  $10^{-5}$ .

All simulations are run on a desktop (13th Intel(R) i7 CPU@2.10GHz) and QP is solved using the ‘‘mosek’’ solver with the interior-point-convex algorithm in MATLAB.

### A. Performance Metrics

We assess the performance of the swarm according to five different metrics.

- Total runtime  $t$ : The total execution time excluding the offline data preparation phase. The total time is set to be infinite when the swarm transport task cannot be completed within the maximum terminal time step  $T_f^{max} = 3000$ .
- Runtime per time step  $t_f$ : The total runtime divided by the total number of time steps. This metric reflects the computational efficiency when the discretization time intervals are uniform.
- Average trajectory length  $\bar{D}$ : The average of the agents’ traversed distances until they reach the target area. This value is set to infinite when any robot fails to arrive at the goal position.
- Minimum inter-robot distance  $\min(d_{ij})$ : The minimum distance among neighboring robots over the whole trajectory.
- Minimum distance to obstacles  $\min(d_{io})$ : The minimum distance between all agents and all obstacles over the transport mission.

### B. Adaptability to Different Environments

We compared the performance of our method ROVER in different scenarios with several state-of-art approaches. Benchmark approaches highly pertinent to our research include multi-robot Formation Control (Formation Control) [21], Predictive Control of aerial swarms (Predictive Control) [11], and Optimal Tube swarm planning and control (Optimal Tube) [22]. However, Optimal Tube [22] proves impractical for our swarm transport task. Our swarm is partitioned into distinct subgroups for various goal areas concerning variation in swarm density, which cannot be accomplished with a single virtual tube planning as mentioned in the article.

Therefore, the following section presents a comparative analysis between our method and the remaining two benchmark approaches.

All approaches are tested with various robot numbers in three typical scenarios with varying complexity as shown in Fig. 1, including a simple scenario composed of uniformly distributed circular obstacles (scenario 1), a scenario consisting of large polygonal obstacles (scenario 2), and the most complex one characterized by a large number of fragmented polygonal obstacles (scenario 3).

The trajectories composed of the robot's position at each discrete time step generated by different approaches are illustrated in Fig. 1, demonstrating the performance of different approaches.

ROVER and Predictive Control allow the swarm to split and merge when encountering obstacles, while Formation Control constrains the swarm to travel in a group. As hierarchical approaches, ROVER and Formation Control yield considerably varied swarm behaviors. ROVER adopts GMM as a description of the swarm at the planning level. The adaptive change of GCs and their corresponding weights in the GMM enables the swarm's split and merge, which results in likewise flexibility of the swarm as provided by the microscopic method Predictive Control. In contrast, Formation Control involves the sampling of a formation sequence at the planning level to transform the swarm into the target formation, which confines robots within the same formation and thereby sacrifices flexibility.

Table I presents a quantitative comparison of different approaches, where each of the three results is generated by ROVER / Formation Control / Predictive Control, respectively.

As the complexity of the scenarios increases,  $t$  and  $t_f$  of all three methods illustrate an upward trend, where ROVER still demonstrates a significant advantage computation speed. In terms of  $\bar{D}$ , Predictive Control maintains a stable and shortest path across all three scenarios because Predictive Control optimizes every robot's path individual with fixed start and goal positions. Formation exhibit increasing and largest  $\bar{D}$ , as finding a formation sequence that can accommodate all robots becomes incrementally challenging in more complex scenarios. ROVER's  $\bar{D}$  also grows with scene complexity but falls between the other two algorithms, aligning with the flexibility of ROVER produced by the split and merge performance as shown in Fig. 1. For  $\min(d_{ij})$  and  $\min(d_{io})$ , ROVER's result are positively correlated with the width of the passages in the map, while Formation Control maintains a larger distance from obstacles, but sacrificing  $\min(d_{ij})$  and increasing  $\bar{D}$ . Furthermore, Predictive Control adopts soft constraints for obstacle avoidance, resulting in collisions in all three scenarios with 500 robots.

### C. Risk-Aware Planning with Different Risk Acceptance Levels

To assess the risk control capability of ROVER, which surpasses other approaches discussed earlier, we analyze the swarm behavior under different  $\alpha$ 's. This comparison

involved setting  $\alpha$ 's to 0.05, 0.15 and 0.3 in scenario 2 with 500 robots. We conducted a comprehensive analysis of the minimum distances maintained by all robots from obstacles throughout their entire motion trajectory. Specifically, we selected the closest 30% of robots to the obstacles, which predominantly clustered along the periphery of the robot swarm. Subsequently, a frequency distribution histogram Fig. 2 is constructed to depict the minimum distance observed among these 150 robots. The histograms clearly illustrate how varying risk acceptance levels can effectively modulate the proximity of a robot swarm to obstacles. Notably, lower values of  $\alpha$  lead to more cautious, risk-averse trajectories, ensuring greater distances between the robots and obstacles, which also results in an increase in computational time, distance-to-go, and energy expenditure as illustrated in Tab. II. Specifically, when traversing narrow passages between obstacles, some robots must wait for the remaining robots to pass through before entering the confined space under a small  $\alpha$ , in order to maintain a certain distance from the obstacles. This waiting period contributes to an augmented time consumption. Additionally, a smaller  $\alpha$  systematically prompts the swarm to select paths further away from obstacles when circumventing obstacles, ultimately resulting in longer trajectories and higher energy consumption.

## V. CONCLUSION AND FUTURE WORK

In this work, we propose ROVER under a FTMPC framework. The hierarchical planning strategy and GMM representation of the swarm bring a great flexibility of ROVER, allowing the robot swarm to split and merge to travel around obstacles. Furthermore, ROVER demonstrates high scalability. Leveraging the properties of GMM-CVaR and sequential optimization techniques allow ROVER to provide online motion planning for large-scale swarm robotic systems comprising hundreds or thousands of robots. Nevertheless, utilizing CVaR enables effective management of the proximity of the swarm and obstacles, ensuring a safe navigation through cluttered environments. Extensive comparison in simulation has illustrated the remarkable effectiveness of ROVER in terms of flexibility, scalability, and risk mitigation.

Future work entails extending ROVER to unknown environments and evaluating our methodology through real-world experiments.

## REFERENCES

- [1] M. Brambilla, E. Ferrante, M. Birattari, and M. Dorigo, "Swarm robotics: a review from the swarm engineering perspective," *Swarm Intelligence*, vol. 7, pp. 1–41, 2013.
- [2] E. Tuci, M. H. Alkilabi, and O. Akanyeti, "Cooperative object transport in multi-robot systems: A review of the state-of-the-art," *Frontiers in Robotics and AI*, vol. 5, p. 59, 2018.
- [3] R. Groß and M. Dorigo, "Towards group transport by swarms of robots," *International Journal of Bio-Inspired Computation*, vol. 1, no. 1-2, pp. 1–13, 2009.
- [4] G. Bevacqua, J. Cacace, A. Finzi, and V. Lippiello, "Mixed-initiative planning and execution for multiple drones in search and rescue missions," in *Proceedings of the International Conference on Automated Planning and Scheduling*, vol. 25, pp. 315–323, 2015.

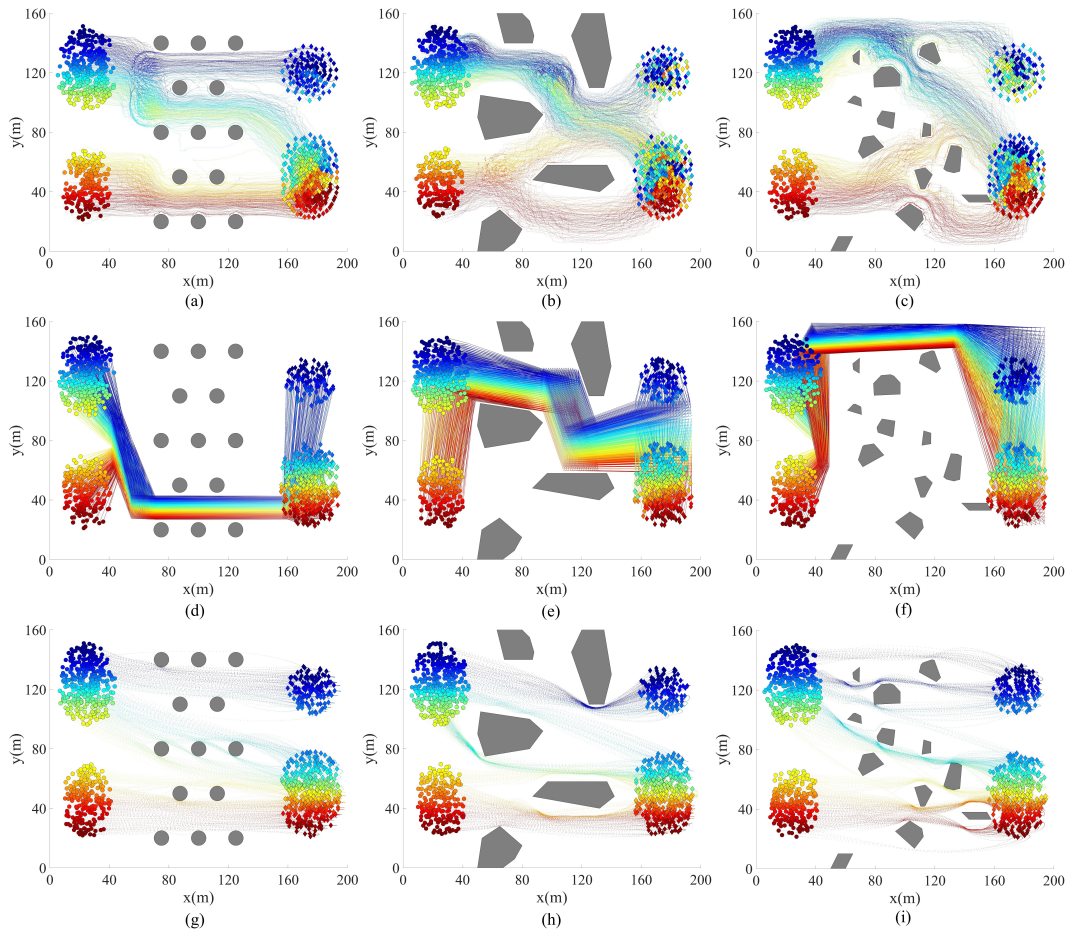


Fig. 1. Figure (a)-(c), (d)-(f), and (g)-(i) show the trajectories of the swarm with 500 robots generated by ROVER, Formation Control, and Predictive Control, respectively. The initial positions of robots are demonstrated by circles, while their corresponding final positions are highlighted by diamonds. The gray polygons represent static obstacles in the workspace. Scenario 1, 2 and 3 are arranged from left to right, respectively.

TABLE I  
NUMERICAL COMPARISON OF THE APPROACHES WITH 500 ROBOTS

Scenario	$t(\text{min})$	$t_f(\text{s})$	$\bar{D}(\text{m})$	$\min(d_{ij})(\text{m})$	$\min(d_{io})(\text{m})$
1	4.28 / 41.35 / 66.60	0.54 / 1.23 / 21.37	170.05 / 269.40 / 160.11	0.32 / 0.23 / 0.078	0.49 / 1.96 / -0.45
2	5.44 / 44.51 / 116.76	0.57 / 1.26 / 29.81	198.67 / 279.70 / 162.09	0.62 / 0.23 / 0.02	0.76 / 7.00 / -6.57
3	6.05 / 58.58 / 120.78	0.64 / 1.28 / 31.51	202.26 / 364.16 / 159.03	0.58 / 0.23 / 0.03	0.34 / 6.80 / -2.96

TABLE II  
NUMERICAL COMPARISON UNDER DIFFERENT  $\alpha$ 's

$\alpha$	$t(\text{min})$	$\bar{D}(\text{m})$
0.05	5.50	191.0
0.15	4.20	174.6
0.3	3.81	173.2

[5] K. Cui, M. Li, C. Fabian, and H. Koepl, "Scalable task-driven robotic swarm control via collision avoidance and learning mean-field control," in *2023 IEEE International Conference on Robotics and Automation (ICRA)*, pp. 1192–1199, IEEE, 2023.

[6] K. Zhang, Z. Yang, and T. Başar, "Multi-agent reinforcement learning: A selective overview of theories and algorithms," *Handbook of reinforcement learning and control*, pp. 321–384, 2021.

[7] T. Chu, J. Wang, L. Codecà, and Z. Li, "Multi-agent deep reinforcement learning for large-scale traffic signal control," *IEEE Transactions on Intelligent Transportation Systems*, vol. 21, no. 3, pp. 1086–1095, 2019.

[8] L. Streichenberg, E. Trevisan, J. J. Chung, R. Siegwart, and J. Alonso-Mora, "Multi-agent path integral control for interaction-aware motion planning in urban canals," *arXiv preprint arXiv:2302.06547*, 2023.

[9] M. A. Pereira, A. D. Saravanos, O. So, and E. A. Theodorou, "Decentralized safe multi-agent stochastic optimal control using deep fbsdes and adm," *arXiv preprint arXiv:2202.10658*, 2022.

[10] J. Yin, Z. Zhang, E. Theodorou, and P. Tsiotras, "Trajectory distribution control for model predictive path integral control using covariance steering," in *2022 International Conference on Robotics and Automation (ICRA)*, pp. 1478–1484, IEEE, 2022.

[11] E. Soria, F. Schiano, and D. Floreano, "Predictive control of aerial swarms in cluttered environments," *Nature Machine Intelligence*, vol. 3, no. 6, pp. 545–554, 2021.

[12] E. Soria, F. Schiano, and D. Floreano, "Distributed predictive drone



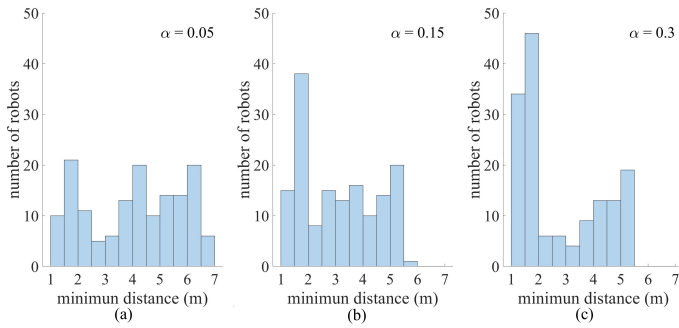


Fig. 2. Figures (a)-(c) show the number of robots in different minimum  $d_{i_0}$  intervals throughout the entire trajectory, where  $\alpha$  equals 0.05, 0.15, and 0.3 respectively.

swarms in cluttered environments,” *IEEE Robotics and Automation Letters*, vol. 7, no. 1, pp. 73–80, 2021.

- [13] K. Elamvazhuthi and S. Berman, “Mean-field models in swarm robotics: A survey,” *Bioinspiration & Biomimetics*, vol. 15, no. 1, p. 015001, 2019.
- [14] T. Zheng, Q. Han, and H. Lin, “Transporting robotic swarms via mean-field feedback control,” *IEEE Transactions on Automatic Control*, vol. 67, no. 8, pp. 4170–4177, 2021.
- [15] Y. Chen, “Density control of interacting agent systems,” *IEEE Transactions on Automatic Control*, 2023.
- [16] S. Ma, M. Hou, X. Ye, and H. Zhou, “High-dimensional optimal density control with wasserstein metric matching,” in *2023 62nd IEEE Conference on Decision and Control (CDC)*, pp. 6813–6818, IEEE, 2023.
- [17] V. Krishnan and S. Martínez, “Distributed optimal transport for the deployment of swarms,” in *2018 IEEE Conference on Decision and Control (CDC)*, pp. 4583–4588, IEEE, 2018.
- [18] S. Biswal, K. Elamvazhuthi, and S. Berman, “Decentralized control of multiagent systems using local density feedback,” *IEEE Transactions on Automatic Control*, vol. 67, no. 8, pp. 3920–3932, 2021.
- [19] P. Zhu, C. Liu, and S. Ferrari, “Adaptive online distributed optimal control of very-large-scale robotic systems,” *IEEE Transactions on Control of Network Systems*, vol. 8, no. 2, pp. 678–689, 2021.
- [20] A. D. Saravanos, Y. Li, and E. A. Theodorou, “Distributed hierarchical distribution control for very-large-scale clustered multi-agent systems,” *arXiv preprint arXiv:2305.18718*, 2023.
- [21] J. Alonso-Mora, S. Baker, and D. Rus, “Multi-robot formation control and object transport in dynamic environments via constrained optimization,” *The International Journal of Robotics Research*, vol. 36, no. 9, pp. 1000–1021, 2017.
- [22] P. Mao, R. Fu, and Q. Quan, “Optimal virtual tube planning and control for swarm robotics,” *arXiv preprint arXiv:2304.11407*, 2023.
- [23] M. Ono, M. Pavone, Y. Kuwata, and J. Balaram, “Chance-constrained dynamic programming with application to risk-aware robotic space exploration,” *Autonomous Robots*, vol. 39, pp. 555–571, 2015.
- [24] A. Wang, A. Jasour, and B. C. Williams, “Non-gaussian chance-constrained trajectory planning for autonomous vehicles under agent uncertainty,” *IEEE Robotics and Automation Letters*, vol. 5, no. 4, pp. 6041–6048, 2020.
- [25] D. D. Fan, K. Otsu, Y. Kubo, A. Dixit, J. Burdick, and A.-A. Agha-Mohammadi, “Step: Stochastic traversability evaluation and planning for risk-aware off-road navigation,” in *Robotics: Science and Systems*, pp. 1–21, RSS Foundation, 2021.
- [26] M. Norton, V. Khokhlov, and S. Uryasev, “Calculating cvar and bpoe for common probability distributions with application to portfolio optimization and density estimation,” *Annals of Operations Research*, vol. 299, pp. 1281–1315, 2021.
- [27] A. Hakobyan, G. C. Kim, and I. Yang, “Risk-aware motion planning and control using cvar-constrained optimization,” *IEEE Robotics and Automation Letters*, vol. 4, no. 4, pp. 3924–3931, 2019.
- [28] A. Hakobyan and I. Yang, “Distributionally robust risk map for learning-based motion planning and control: A semidefinite programming approach,” *IEEE Transactions on Robotics*, 2022.
- [29] A. Zolanvari and A. Cherukuri, “Data-driven distributionally robust

iterative risk-constrained model predictive control,” in *2022 European Control Conference (ECC)*, pp. 1578–1583, IEEE, 2022.

- [30] C. Villani, *Topics in optimal transportation*, vol. 58. American Mathematical Soc., 2021.
- [31] Y. Chen, T. T. Georgiou, and A. Tannenbaum, “Optimal transport for gaussian mixture models,” *IEEE Access*, vol. 7, pp. 6269–6278, 2018.
- [32] E. G. Gilbert, D. W. Johnson, and S. S. Keerthi, “A fast procedure for computing the distance between complex objects in three-dimensional space,” *IEEE Journal on Robotics and Automation*, vol. 4, no. 2, pp. 193–203, 1988.
- [33] G. Van Den Bergen, “Proximity queries and penetration depth computation on 3d game objects,” in *Game Developers Conference*, vol. 170, 2001.
- [34] R. T. Rockafellar and S. Uryasev, “Conditional value-at-risk for general loss distributions,” *Journal of banking & finance*, vol. 26, no. 7, pp. 1443–1471, 2002.
- [35] P. Zhu, S. Ferrari, J. Morelli, R. Linares, and B. Doerr, “Scalable gas sensing, mapping, and path planning via decentralized hilbert maps,” *Sensors*, vol. 19, no. 7, p. 1524, 2019.
- [36] X. Yang, H. Gao, P. Zhu, and C. Liu, “Risk-aware motion planning for very-large-scale robotics systems using conditional value-at-risk,” in *International Conference on Intelligent Robotics and Applications*, pp. 513–525, Springer, 2023.
- [37] G. Pertaia and S. Uryasev, “Fitting heavy-tailed mixture models with cvar constraints,” *Dependence Modeling*, vol. 7, no. 1, pp. 365–374, 2019.
- [38] J. M. Danskin, *The theory of max-min and its application to weapons allocation problems*, vol. 5. Springer Science & Business Media, 2012.
- [39] F. Facchinei, L. Lampariello, and G. Scutari, “Feasible methods for nonconvex nonsmooth problems with applications in green communications,” *Mathematical Programming*, vol. 164, no. 1-2, pp. 55–90, 2017.

## APPENDIX

### A. Proof of proposition 1

*Proof.* This section is dedicated to building the relationship between the distributions  $\sum_{j=1}^N \omega_j Pr(-sd(\mathbf{X}^j, \mathcal{O}_i))$  and  $Pr(-sd(\mathbf{X}, \mathcal{O}_i))$ . Here we have a signed distance mapping  $sd : \mathcal{X} \subset \mathbb{R}^2 \rightarrow \mathcal{Y} \subset \mathbb{R}$ . Without loss of generality, we omit the obstacle parameter in  $sd$  in the context of considering one static obstacle and define  $Y^j = sd(\mathbf{X}^j, \mathcal{O}_i) = sd(\mathbf{X}^j)$  and  $Y = sd(\mathbf{X}, \mathcal{O}_i) = sd(\mathbf{X})$ . We then define the preimage of  $sd$ , i.e.,  $sd^{-1} : \mathcal{Y} \subset \mathbb{R} \rightarrow \mathcal{X} \subset \mathbb{R}^2$ , such that  $sd^{-1}(\mathcal{Y}) = \{\mathbf{X} \in \mathcal{X} | sd(\mathbf{X}) \in \mathcal{Y}\}$ . We derive the probability  $Pr(Y \in \mathcal{Y})$ , i.e.,

$$Pr(Y \in \mathcal{Y}) = Pr(sd(\mathbf{X}) \in \mathcal{Y}) \quad (24a)$$

$$= \sum_{q=1}^Q Pr(sd(\mathbf{X}) \in \mathcal{Y}_q) \quad (24b)$$

$$= \sum_{q=1}^Q Pr(\mathbf{X} \in sd^{-1}(\mathcal{Y}_q)) \quad (24c)$$

$$= Pr(\mathbf{X} \in sd^{-1}(\mathcal{Y})) \quad (24d)$$

$$= \int_{\mathcal{X}} p(\mathbf{X}) d\mathbf{X} \quad (24e)$$

$$= \int_{\mathcal{X}} \sum_{j=1}^N p(\mathbf{X}|c(\mathbf{X})=j)p(c(\mathbf{X})=j) d\mathbf{X} \quad (24f)$$

$$= \sum_{j=1}^N \int_{\mathcal{X}} p(\mathbf{X}|c(\mathbf{X})=j)p(c(\mathbf{X})=j) d\mathbf{X} \quad (24g)$$

$$= \sum_{j=1}^N \int_{\mathcal{X}} p(\mathbf{X}|c(\mathbf{X})=j)\omega_j d\mathbf{X} \quad (24h)$$

$$= \sum_{j=1}^N \omega_j \int_{\mathcal{X}} p(\mathbf{X}|c(\mathbf{X})=j) d\mathbf{X} \quad (24i)$$

$$= \sum_{j=1}^N \omega_j Pr(sd^{-1}(\mathcal{Y})|c(\mathbf{X})=j) \quad (24j)$$

$$= \sum_{j=1}^N \omega_j Pr(Y^j \in \mathcal{Y}). \quad (24k)$$

Due to the local monotonicity of  $sd(\cdot)$ , eq. (24b) can be derived into eq. (24c) for each monotonic interval. As there exists a finite number of extrema in  $sd(\cdot)$ , eq. (24a) to eq. (24d) can be established. The derivation to eq. (24e) holds because of the continuity of  $sd(\cdot)$ . As  $\mathcal{Y}$  is a Borel set, the  $sd^{-1}(\mathcal{Y})$  is also measurable. Derivation from eq. (24e) to eq. (24f) is based on the definition of GMM and Bayes' theorem, with  $c(\mathbf{X}) = j$  representing the event that  $\mathbf{X}$  is sampled from the  $j$ th GC. The reasoning from eq. (24i) to eq. (24k) involves the SDF defined under Gaussian uncertainty.  $\square$

### B. Proof of proposition 2

*Proof.* According to the definition of CVaR in eq. (7) and the general properties of GMM,  $CVaR_\alpha(Y)$  can be defined as

$$CVaR_\alpha(Y) = \min_{z \in \mathbb{R}} \mathbb{E} \left[ z + \frac{[Y - z]^+}{\alpha} \right] \quad (25a)$$

$$= \min_{z \in \mathbb{R}} \left[ z + \int_z^{+\infty} \frac{y - z}{\alpha} p(Y) dy \right] \quad (25b)$$

$$= \min_{z \in \mathbb{R}} \left[ z + \int_z^{+\infty} \frac{y - z}{\alpha} \sum_{j=1}^N \omega_j p(Y^j) dy \right], \quad (25c)$$

where  $p(\cdot)$  denotes the PDF of a random variable. For notation simplicity, we define

$$Q(\boldsymbol{\omega}, z) = z + \int_z^{+\infty} \frac{y - z}{\alpha} \sum_{j=1}^N \omega_j p(Y^j) dy, \quad (26)$$

where  $\boldsymbol{\omega} = [\omega_1, \omega_2, \dots, \omega_N]$ , and thus we obtain

$$CVaR_\alpha(Y) = \min_{z \in \mathbb{R}} Q(\boldsymbol{\omega}, z). \quad (27)$$

By taking the partial derivative of  $Q(\boldsymbol{\omega}, z)$  concerning  $z$  as

$$\frac{\partial Q(\boldsymbol{\omega}, z)}{\partial z} = 1 - \int_z^{+\infty} \frac{p(Y)}{\alpha} dy, \quad (28)$$

and leveraging the monotonicity of CDF, we can obtain the minimizer

$$z^* = \arg \min_{z \in \mathbb{R}} Q(\boldsymbol{\omega}, z) = VaR_\alpha(Y), \quad (29)$$

based on the definition of VaR.

Plugging  $z^*$  into eq. (25c), the  $CVaR_\alpha(Y)$  can be further derived as follows:

$$\begin{aligned} CVaR_\alpha(Y) &= VaR_\alpha(Y) + \int_{VaR_\alpha(Y)}^{+\infty} \frac{y - VaR_\alpha(Y)}{\alpha} \sum_{j=1}^N \omega_j p(Y^j) dy \quad (30a) \\ &= VaR_\alpha(Y) + \frac{1}{\alpha} \sum_{j=1}^N \omega_j \left[ \int_{VaR_\alpha(Y)}^{+\infty} yp(Y^j) dy - \alpha_j VaR_\alpha(Y) \right] \quad (30b) \end{aligned}$$

$$= \frac{1}{\alpha} \sum_{j=1}^N \omega_j \int_{VaR_\alpha(Y)}^{+\infty} yp(Y^j) dy \quad (30c)$$

$$= \frac{1}{\alpha} \sum_{j=1}^N \omega_j \alpha_j CVaR_{\alpha_j}(Y^j). \quad (30d)$$

To obtain eqs. (30b) and (30c), we define an auxiliary variable  $\alpha_j$  as

$$\alpha_j = \int_{VaR_\alpha(Y)}^{+\infty} p(Y^j) dy, \quad (31a)$$

$$\alpha = \sum_{j=1}^N \omega_j \alpha_j, \quad (31b)$$

which refers to the tail probability of the  $j$ th Gaussian SDF distribution at the  $VaR_\alpha(Y)$  quantile. The transformation to eq. (30d) is based on the relationship of CVaR and VaR given in eq. (7).  $\square$

### C. Derivation of gradient of GMM-CVaR

According to the Danskin's theorem [38],  $CVaR_\alpha(Y)$  defined by eq. (27) is differentiable w.r.t.  $\boldsymbol{\omega}$ , since  $z^*$  is the unique minimizer of  $Q(\boldsymbol{\omega}, z)$  as shown in eq. (29). And the partial derivatives can be computed by

$$\frac{\partial CVaR_\alpha(Y)}{\partial \omega_j} = \left. \frac{\partial Q(\boldsymbol{\omega}, z)}{\partial \omega_j} \right|_{z=VaR_\alpha(Y)} \quad (32a)$$

$$= \frac{1}{\alpha} \int_{VaR_\alpha(Y)}^{+\infty} yp(Y^j) dy - \frac{VaR_\alpha(Y)}{\alpha} \int_{VaR_\alpha(Y)}^{+\infty} p(Y^j) dy \quad (32b)$$

$$= \frac{\alpha_j}{\alpha} CVaR_{\alpha_j}(Y^j) - \frac{\alpha_j}{\alpha} VaR_\alpha(Y). \quad (32c)$$

The transformation from eq. (32b) to eq. (32c) leverages the relationship of CVaR and VaR given in eq. (7).